Int. J. Heat Mass Transfer. Vol. 36, No. 13, pp. 3159–3170, 1993
Printed in Great Britain

0017–9310/93 $6.00 + 0.00

Transient natural convection heat transfer between concentric spheres

HSIN-SEN CHU and TZONG-SHING LEE
Department of Mechanical Engineering, National Chiao Tung University, Hsinchu, Taiwan 30050, R.O.C.

(*Received* 19 *August* 1992 *and in final form* 3 *March* 1993)

Abstract—The transient laminar natural convection heat transfer of fluids between two concentric isothermal spheres is investigated theoretically. The fluid is initially at rest and then the inner wall is subjected to a step change of temperature. The stream function/vorticity formulation is employed for the analysis because of the symmetry of the problem. The transient behavior of the flow field and its subsequent effect on the temperature distribution for different Rayleigh numbers and radius ratios are analyzed by finite difference methods. Forward differences are used for the time derivatives and second-order central differences for the space derivatives. The alternating direction implicit method is used for solution of the discretization equations. The results show that the Rayleigh number and radius ratio have a profound influence on the temperature and flow fields. The results of average Nusselt numbers are also compared with those of previous experimental and numerical investigations. Excellent agreement is obtained.

INTRODUCTION

NATURAL convection heat transfer in the annulus between two concentric spheres is an important research topic, because this geometry is encountered in a wide range of engineering design problems. Examples include nuclear reactor design, thermal energy storage cells that utilize phase transition, solar energy collectors, geophysical fields, and many other practical situations. Accurate prediction of steady state heat transfer rates and temperature distribution is required in these engineering design problems. For some engineering applications, such as gyroscopes, the prediction of transient temperature distribution and heat transfer rate from initial state to steady state is very important. Unfortunately, little of the literature published in the past two decades investigates the transient behavior of laminar natural convection occuring in the annuli between two concentric spheres.

Experimental research on natural convection in annuli between two isothermal concentric spheres has been described by Bishop *et al.* [1, 2], Scanlan *et al.* [3], and Yin *et al.* [4]. Three types of flow patterns in the annuli between the concentric spheres were observed for various radius ratios, Prandtl numbers, and Rayleigh numbers. These were crescent eddies, kidney-shaped flows, and falling-vortices.

The analytical investigation of natural convection in annuli between two isothermal concentric spheres, the inner surface being hotter, was initiated by Mack and Hardee [5], who developed a regular perturbation method to determine the temperature and flow fields. The streamlines and isotherms were displayed graphically. Local and overall Nusselt numbers were also presented and compared with those obtained experimentally. Later, a finite-difference scheme was used by Brown [6], who extended this problem to include a much larger range of Prandtl and Grashof numbers. Shaughnessy *et al.* [7] used the spectral expansions technique to solve nonlinear partial differential equations that govern the problem of natural convection heat transfer between concentric horizontal cylinders and concentric spherical annuli. They concluded that their methods were valid for a greater range of parameter values than can be solved by perturbation methods. But the range of Rayleigh numbers for which accurate solutions can be obtained was very limited. Astill *et al.* [8] solved this problem for Prandtl numbers between 0.7 and 5.0 by using the finite-difference method. Their results cover a range of $Ra = 5.0 \times 10^1$–2.0×10^9 for radius ratios from 1.03 to 2.0. Other solutions of the problem which deal with natural convection in spherical annuli with uniform wall temperatures have been presented in refs. [9–15].

All the references cited above have dealt with steady-state analyses only. Recent work concerning transient behavior in spherical annuli is presented in refs. [16–19]. Ozoe *et al.* [16] and Mochimaru [17] studied transient natural convection in a spherical/hemispherical enclosure after a step change in the spherical wall temperature experimentally and numerically. Fujii *et al.* [18] obtained a numerical solution of full Navier–Stokes and energy equations for two-dimensional laminar natural convection in spherical annuli between two concentric spheres for large radius ratio at Prandtl number of 0.7 and Rayleigh number of 100. Later, they extended the problem for large Prandtl number, $Pr = 0.7$–120 [20]. Ozoe *et al.* [19] presented a full three-dimensional numerical analysis of natural convection in a spherical annuli

NOMENCLATURE

C_p	specific heat at constant pressure
g	local gravitational acceleration [m s^{-2}]
Gr	Grashof number, $(g\beta\Delta T r_i^3)/\nu^2$
k	thermal conductivity of the fluid [W m^{-1} K^{-1}]
Nu_i	local Nusselt number at inner sphere surface, defined by equation (10)
Nu_o	local Nusselt number at outer sphere surface, defined by equation (11)
$\overline{Nu_i^*}$	average Nusselt number at inner sphere surface, defined by equation (12)
$\overline{Nu_o^*}$	average Nusselt number at outer sphere surface, defined by equation (12)
Pr	Prandtl number, ν/α
r	radial coordinate
r_i	radius of inner sphere
r_o	radius of outer sphere
R	dimensionless radial coordinate, r/r_i
R^*	ratio of outer and inner radius ratio, r_o/r_i
Ra	Rayleigh number, $(g\beta\Delta T r_i^3)/(\nu\alpha)$
t	time [s]
T	non-dimensional temperature, $(T'-T'_o)/(T'_i-T'_o)$
T'	temperature
T'_i	temperature of inner sphere
T'_o	temperature of outer sphere and initial state
U	non-dimensional radial velocity, ur_i/α
u	radial velocity
V	non-dimensional tangential velocity, vr_i/α
v	tangential velocity.

Greek symbols

α	thermal diffusivity, $k/C_p\rho$
β	thermal expansion coefficient
ΔT	temperature difference between spheres, $T'_i-T'_o$
θ	angular coordinate measured positive clockwise from upper vertical line of symmetry $\theta = 0^\circ$
θ^*	angular position at vortex center
ν	kinematic viscosity
ρ	fluid density
τ	non-dimensional time, $\alpha t/r_i^2$
Ψ	non-dimensional stream function, $\Psi'/\alpha r_i$
Ψ'	stream function in spherical coordinates
ω	vorticity
Ω	non-dimensional vorticity, $\omega r_i^2/\alpha$.

Subscripts

i	inner wall
max	maximum value
o	outer wall.

between two concentric spheres under nonsymmetrical thermal boundary conditions. Their work, however, only dealt with $Ra = 500$ and $Pr = 1.0$.

In the present study, transient laminar natural convection between two concentric spheres for a step heating of inner sphere is studied numerically. The complete Navier–Stokes equations are transformed and expressed in terms of vorticity and stream function. The transformed equations, vorticity transport equation, and energy equation are then solved by an alternating direction implicit method (ADI), while the Gaussian successive over-relaxation (SOR) technique is utilized to solve the stream function equation. Transient behavior of the flow and temperature field is displayed graphically. The influence of different Rayleigh numbers and radius ratios on heat transfer rates is also investigated.

ANALYSIS

A schematic diagram of the physical system to be investigated is shown in Fig. 1. The gap between the spheres is filled with a viscous, incompressible Newtonian fluid. It is assumed that the fluid is at rest at a constant temperature T'_o initially. For $t \geq 0$, the inner sphere of radius r_i is kept at a constant temperature T'_i, while the outer sphere of radius r_o is still maintained at T'_o, with $T'_i > T'_o$. The flow is symmetrical about a vertical diameter parallel to the line of gravity acceleration. The mathematical formulation of the problem uses spherical coordinates with the origin at the center of the inner sphere. The angular coordinate is measured in the clockwise direction, with $\theta = 0$ at the top and $\theta = \pi$ at the bottom of the spheres. Furthermore, it is assumed that (1) the fluid properties are constant except for the density variation with temperature in the buoyancy term, i.e. the Boussinesq approximation is valid, and (2) viscous dissipation and radiation effects can be neglected.

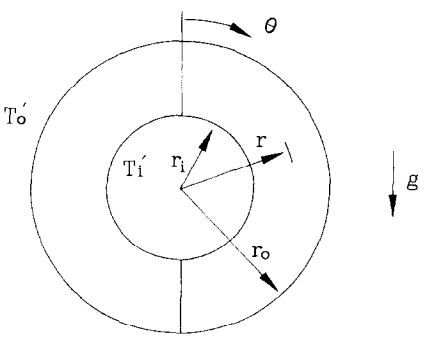

FIG. 1. Physical model and coordinate system.

The flow field inside the annulus is conveniently described by the Navier–Stokes equations. Since the problem is two-dimensional due to the axisymmetry and the fact that the vorticity vector reduces to a scalar quantity, the stream function/vorticity formulation can be employed. Putting governing equations into non-dimensional form yields the following:

Vorticity transport equation:

$$\frac{\partial\Omega}{\partial\tau}+U\left(\frac{\partial\Omega}{\partial R}-\frac{\Omega}{R}\right)+\frac{V}{R}\left(\frac{\partial\Omega}{\partial\theta}-\Omega\cot\theta\right)=Pr\left(\nabla^2-\frac{1}{R^2\sin^2\theta}\right)\Omega-Pr\,Ra\left(\sin\theta\frac{\partial T}{\partial R}+\frac{\cos\theta}{R}\frac{\partial T}{\partial\theta}\right) \quad (1)$$

Stream function equation:

$$\frac{\partial^2\Psi}{\partial R^2}+\frac{1}{R^2}\frac{\partial^2\Psi}{\partial\theta^2}-\frac{\cot\theta}{R^2}\frac{\partial\Psi}{\partial\theta}=\Omega R\sin\theta. \quad (2)$$

Velocities:

$$U=-\frac{1}{R^2\sin\theta}\frac{\partial\Psi}{\partial\theta};\quad V=\frac{1}{R\sin\theta}\frac{\partial\Psi}{\partial R}. \quad (3)$$

The temperature field is described by the transient energy conservation equation in spherical coordinates:

$$\frac{\partial T}{\partial\tau}+U\frac{\partial T}{\partial R}+\frac{V}{R}\frac{\partial T}{\partial\theta}=\nabla^2T \quad (4)$$

where

$$\nabla^2=\frac{1}{R^2}\frac{\partial}{\partial R}\left(R^2\frac{\partial}{\partial R}\right)+\frac{1}{R^2\sin\theta}\frac{\partial}{\partial\theta}\left(\sin\theta\frac{\partial}{\partial\theta}\right). \quad (5)$$

The initial and boundary conditions are given as follows:

for $\tau=0$

$$\Omega=\Psi=\frac{\partial\Psi}{\partial R}=\frac{\partial\Psi}{\partial\theta}=T=0 \quad \text{everywhere}, \quad (6)$$

for $\tau>0$

at $R=1$,

$$\Psi=0,\quad \Omega=\frac{1}{\sin\theta}\frac{\partial^2\Psi}{\partial R^2},\quad T=1; \quad (7)$$

at $R=R^*$,

$$\Psi=0,\quad \Omega=\frac{1}{R^*\sin\theta}\frac{\partial^2\Psi}{\partial R^2},\quad T=0; \quad (8)$$

at $\theta=0,\pi$,

$$\Psi=\Omega=\frac{\partial T}{\partial\theta}=0. \quad (9)$$

The local Nusselt number can be obtained from the gradient of the temperature at the inner and outer boundary from the following relationship:

$$Nu_i=-\frac{R^*-1}{R^*}\left(\frac{\partial T}{\partial R}\right)_{R=1} \quad (10)$$

$$Nu_o=-R^*(R^*-1)\left(\frac{\partial T}{\partial R}\right)_{R=R^*}. \quad (11)$$

The average Nusselt numbers are defined as:

$$\overline{Nu_{i,o}^*}=-\int_0^{\pi}Nu_{i,o}\left[\left(\frac{\sin\theta}{2}\right)\right]d\theta. \quad (12)$$

NUMERICAL METHOD

The vorticity transport, energy transport, and stream function equations together with the initial and boundary conditions provide a complete description of the problem. Since the flow is known to be parabolic in time but elliptic in space, the solution for the problem can only be marched in time. In this study, the time-dependent vorticity transport and energy transport equations were solved by employing the alternating direction implicit (ADI) finite difference technique [21], while the stream function equation was solved by employing the Gaussian successive over-relaxation (SOR) technique [22, 23]. The first and second derivatives in space were approximated by central difference while the time derivatives were approximated by forward difference. Derivatives at the boundaries were approximated by a three-point forward or backward difference. In this study, the accuracy of the numerical scheme was checked quite carefully. Essentially, we ensured that the results were both grid- and time-step-size-independent. A 41×41 grid system and 10^{-4} time step were used for most computations in this study.

The solution procedure was initiated by advancing the temperature distribution one time step through the solution of the energy equation. The vorticity equation was then solved. From the solution of the stream function equation the wall vorticities were updated. The procedure was then repeated for a new time step until the following pre-established convergence criterion was satisfied for all field variables:

$$\frac{|\Psi_{new}-\Psi_{old}|_{max}}{|\Psi_{new}|_{max}}\leqslant10^{-4} \quad (13)$$

where the subscripts new and old indicate the present and previous iterative values respectively. A further check on the convergence of the steady-state solution was made by comparing the average Nusselt number for the inner and outer sphere:

$$\frac{|(\overline{Nu_i^*})^{n+1}-(\overline{Nu_i^*})^n|}{|(\overline{Nu_i^*})^{n+1}|}\leqslant10^{-3} \quad (14)$$

$$\frac{|(\overline{Nu_o^*})^{n+1}-(\overline{Nu_i^*})^{n+1}|}{|(\overline{Nu_i^*})^{n+1}|}\leqslant10^{-3} \quad (15)$$

Table 1. Grid test for a typical case with $Pr = 0.7$, $Ra = 1 \times 10^3$, $R^* = 2.0$ at steady state. The results are compared with those of Mack and Hardee [5], Astill *et al.* [8] and Singh and Chen [12]. θ^* is the angular position at vortex center

Time step	Grid size	$\overline{Nu}^*$	Ψ_{max}	θ^*	CPU time
1.0×10^{-4}	11×21	1.143	3.450	81	
	21×21	1.107	3.256	78	11 m 54.78 s
	31×31	1.101	3.218	78	33 m 37.10 s
	41×41	1.099	3.209	81	56 m 21.45 s
	51×51	1.099	3.203	79.2	2 h 26 m 21.23 s
	61×61	1.099	3.199	81	3 h 40 m 03.21 s
5.0×10^{-5}	31×31	1.106	3.218	78	57 m 23.59 s
	41×41	1.099	3.209	81	1 h 40 m 11.74 s
	51×51	1.099	3.203	79.2	3 h 59 m 54.86 s
	Mack and Hardee [5]	1.120	3.210	77	
	Astill *et al.* [8]	1.120	3.490	79	
	Singh and Chan [12]	1.101			

where the superscripts n and $(n+1)$ indicate the nth and $(n+1)$th time step, respectively.

RESULTS AND DISCUSSION

To check the validity of the numerical results, test calculations were performed for the following values of the controlling parameters: $Pr = 0.7$, $Ra = 1000$, and $R^* = 2.0$. These values are convenient for comparison with earlier work by Mack and Hardee [5], Astill *et al.* [8], and Singh and Chen [12]. The results of the test calculations are displayed in Table 1. Examining Table 1 shows that smaller grid sizes achieve better accuracy but use up more computer time. Since the smaller step sizes of 51×51 and 61×61 did not cause significant changes in the magnitude of the average Nusselt number for the test cases, a uniform grid system of 41×41 was chosen for the calculation of all cases in this study. Numerical test calculations were also performed for different time steps. It was found that a time step of 10^{-4} would give a time-independent solution.

In this work, calculations were carried out for radius ratios of 1.2, 1.5, and 2.0 at Prandtl numbers of 0.7. Rayleigh numbers were varied from the conduction dominated mode into the laminar free convection dominated region. The maximum Rayleigh number was limited by numerical convergence, which in turn was dependent on the radius ratio. The limits of the Rayleigh number for various radius ratios are given in Table 2. The results for steady Nusselt number $\overline{Nu}^*$ and Ψ_{max} are also displayed in Table 3.

Figure 2 presents a series of streamline configurations, isotherms, and velocity vectors for radius ratio of 2.0, Prandtl number of 0.7, and Rayleigh number of 10^3; Fig. 3 presents a corresponding series for Rayleigh number of 10^5. This series of results is designed to show the individual influence of the Rayleigh number of the flow field. In Fig. 2, the streamlines and isotherms are displayed on the left-hand side and the velocity fields are displayed on the right-hand side. For the conditions selected in Fig. 2—radius ratio of 2.0, Rayleigh number of 1000, and Prandtl number of 0.7—the maximum value of stream function $\Psi_{max} = 3.209$ lies at $\theta = 81°$ from the upper vertical line of symmetry and at about the midgap position. The fluid in the close vicinity of the inner sphere has a lower density than that near the outer sphere. Thus, the fluid near the surface of the inner sphere moves upward while the relatively heavy fluid near the outer sphere moves downward. As the fluid moves downward, it loses energy and eventually forces the separation of the thermal boundary layer along the outer sphere. The heavy fluid then enters the thermal boundary layer of the inner sphere and completes the recirculation pattern. At this Rayleigh number, conduction was the dominant mode of heat transfer. The radial and angular components of the velocity field are displayed on the right-hand side. The velocity

Table 2. Rayleigh number ranges for various radius ratios

R^*	Rayleigh number range
1.2	1.0×10^3–3.0×10^6
1.5	1.0×10^2–1.0×10^6
2.0	1.0×10^2–5.0×10^5

Table 3. Average Nusselt number $\overline{Nu}^*$ and Ψ_{max} as functions of Ra and R^*. θ^* is the angular position at vortex center

R^*	Ra	$\overline{Nu}^*$	Ψ_{max}	θ^*
1.2	1.0×10^3	1.000	0.023	90
	1.0×10^4	1.001	0.223	90
	1.0×10^5	1.008	2.273	90
	1.0×10^6	1.361	20.050	81
1.5	1.0×10^2	1.001	0.004	90
	1.0×10^3	1.001	0.388	90
	1.0×10^4	1.073	3.777	85.5
	1.0×10^5	1.917	22.530	76.5
	1.0×10^6	3.708	47.090	58.5
2.0	1.0×10^2	1.001	0.335	90
	1.0×10^3	1.099	3.209	81
	1.0×10^4	1.973	17.280	67.5
	1.0×10^5	3.489	36.530	54
	5.0×10^5	5.378	53.420	49.5

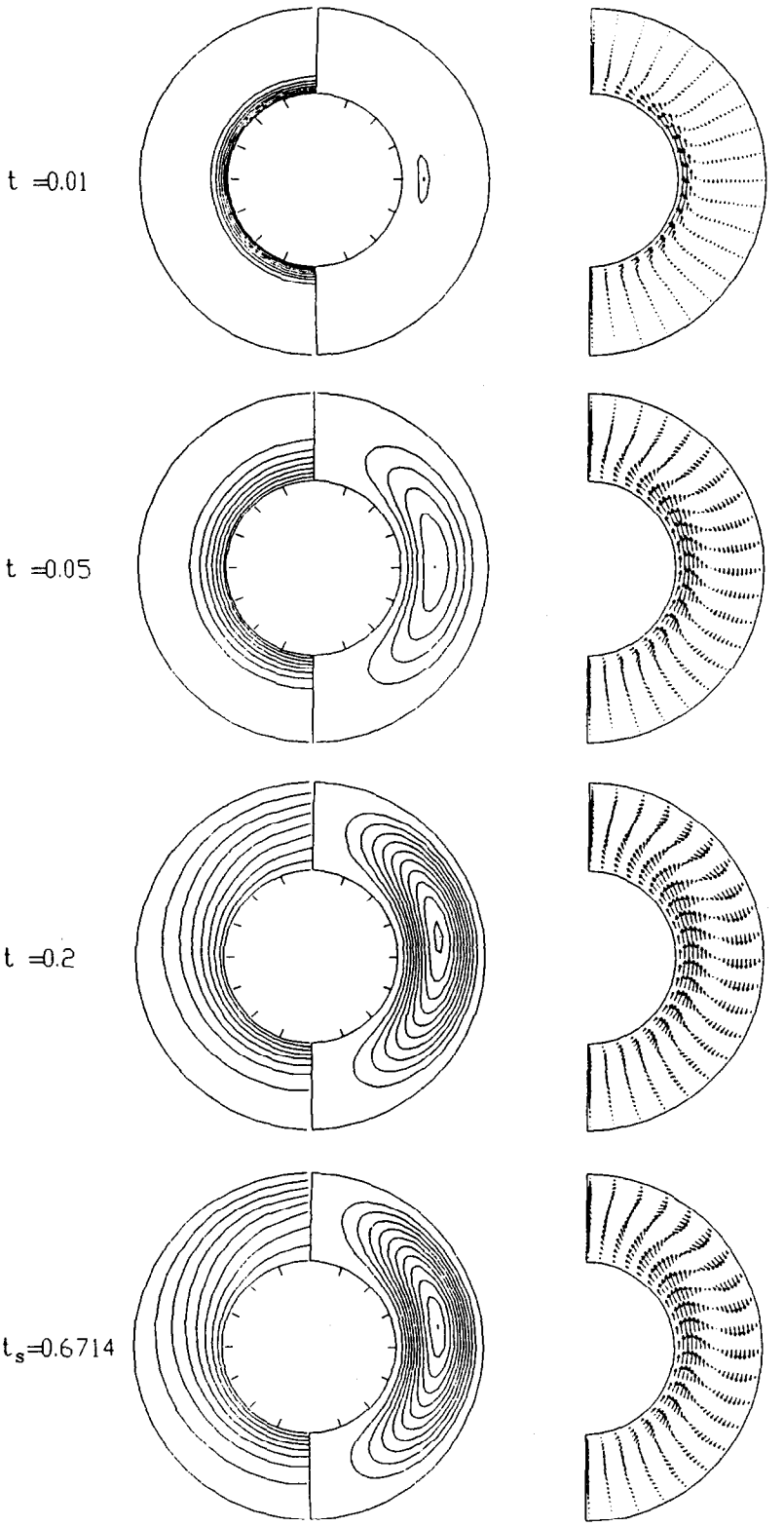

FIG. 2. Streamlines, isotherms, and velocity distributions for $Pr = 0.7$, $Ra = 1.0 \times 10^3$, $R^* = 2.0$ at different time steps. $\Psi_{max} = 3.209$.

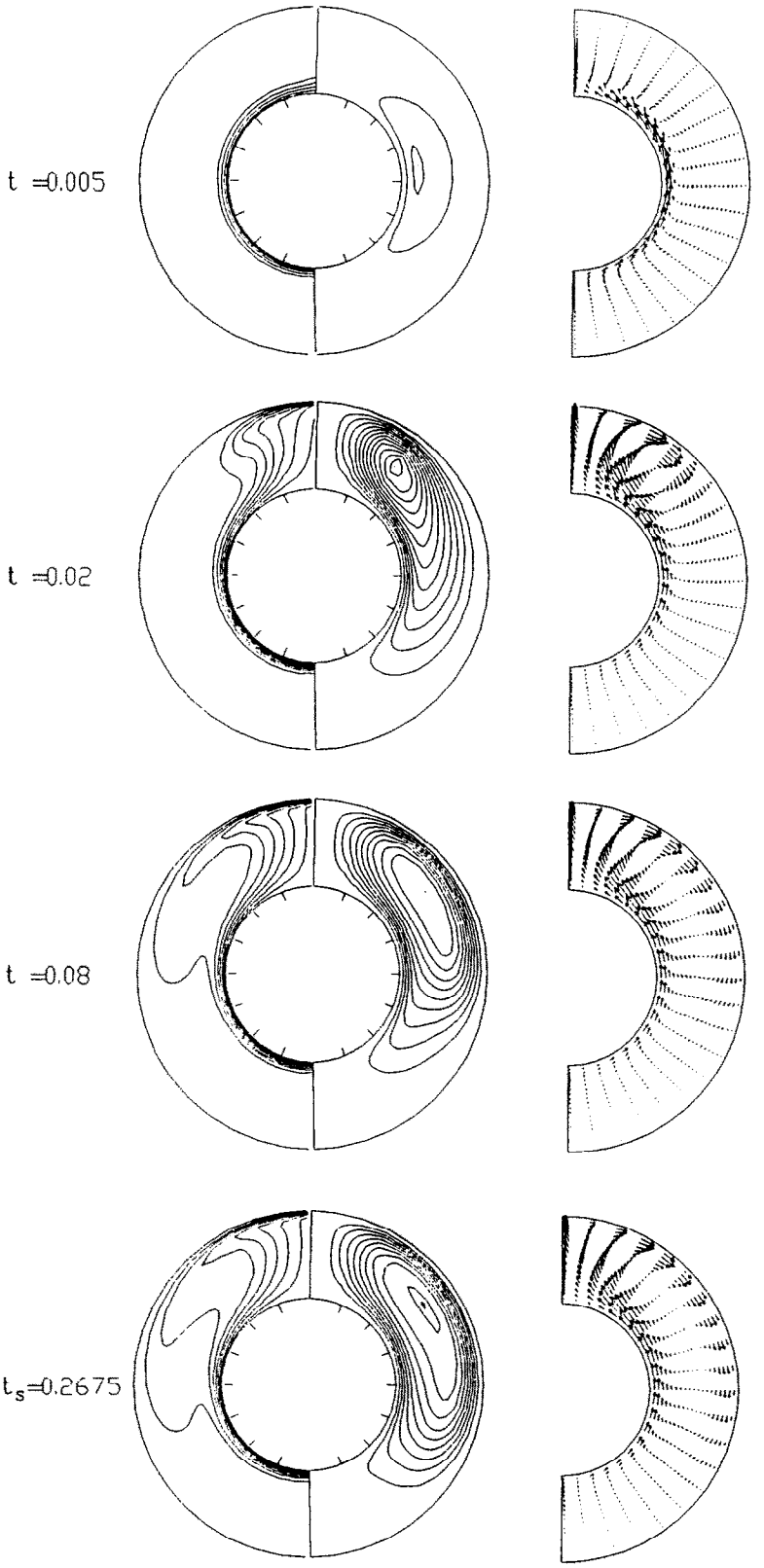

FIG. 3. Streamlines, isotherms, and velocity distributions for $Pr = 0.7$, $Ra = 1.0 \times 10^5$, $R^* = 2.0$ at different time steps. $\Psi_{max} = 36.530$.

vectors were normalized by the maximum local velocity in the flow field and vectors with values of less than 0.01 are not shown in Fig. 2. Both these results and the heat-transfer results are in excellent agreement with the findings of Mack and Hardee [5] for this case. The center of the crescent-shaped eddy stayed close to midgap as variables were changed, but moved into the upper hemisphere as the Rayleigh number increased. This is apparent when we compare the radius ratio of 2.0 in Fig. 2, where the Rayleigh number is 10^3, with that in Fig. 3, where the Rayleigh number is 10^5. For the case of $Ra = 10^5$, laminar convection was the dominant mode of heat transfer and the bottom region was essentially stagnant with low velocities. However, in the top half of the sphere, the fluid was recirculated, making the outer layer warmer. The transport of hot fluid to the outer sphere is also depicted by the isotherms in Figs. 2 and 3. The isotherms exhibit an inversion, and the streamlines are crescent eddy-shaped, as observed by Bishop *et al.* [2].

Figures 4 and 5 show the transient streamlines, isotherms, and velocity distributions for various combinations of $Pr = 0.7$; $Ra = 10^3$ and 10^5; and $R^* = 1.5$. When compared with Figs. 2 and 3, Figs. 4 and 5 show that at fixed Rayleigh number, as the radius ratio increases, the vortex center (the position with the maximum value of the stream function) rises to the upper portion and dips near the $\theta = 90°$ position when the radius is reduced. For a fixed Rayleigh number, the dominant mode of heat transfer will change with a different radius ratio. When the radius ratio is decreased, the dominant mode of heat transfer will be conduction. This result is apparent from comparing Figs. 2 and 4 or Figs. 3 and 5.

Figure 6 demonstrates a set of typical steady temperature distributions for $Pr = 0.7$, $R^* = 2.0$ at $Ra = 10^3$, 10^5, and 5×10^5. Examining Fig. 6, we see that at any radial position, the temperature distribution increases with decreasing θ. For the case where $Ra = 10^3$, the temperature distribution is almost the same as in the pure conduction case. However, at $Ra = 10^5$ and $Ra = 5 \times 10^5$, the natural convection effect is dominant instead of conduction. In the axis of vertical symmetry at $\theta = 0°$, where there is no angular velocity, the temperature continues to decrease slowly in the core along the radial direction until the outer boundary layer is reached, where the temperature falls off sharply once again. At 36°, a temperature inversion appears in the middle of the annulus. Such an inversion is also seen at other angular positions. The fluid in the bottom portion of the annulus is relatively stagnant and stays colder. As expected, the maximum temperature always occurs at the top of the inner sphere for all Rayleigh numbers and diameter ratios. From the difference in temperature distribution between natural convection and conduction, we may calculate the effects of natural convection. In all temperature distribution figures, we also find that the difference in temperature between the profile for 90° and 180° is small, which implies that local heat transfer rates at both inner and outer spheres should be independent of θ.

The transient behavior of the tangential velocity at $\theta = 90°$ for $Pr = 0.7$, $R^* = 2.0$ with $Ra = 10^3$, 10^5, and 5×10^5, respectively, is shown in Fig. 7. Examining this figure we see that the velocity gradients near the inner and outer spheres increase as the Rayleigh number increases from 10^3 to 5×10^5. As expected, the upward and downward flows are still balanced, due to the conservation of mass. For $Ra = 5 \times 10^5$, a two-layer flow structure is observed at $t > 0.04$. The flow formation processes of this particular flow pattern are due to viscous shearing.

The local and average Nusselt numbers for the inner and outer spheres were defined in equations (10)–(12). Since an average Nusselt number of unity represents conduction heat transfer, an average Nusselt number larger than unity indicates the enhancement of heat transfer by free convection. The variation of local Nusselt numbers on the inner sphere and outer sphere at $Ra = 10^3$, $Pr = 0.7$ and $R^* = 2.0$ is shown in Fig. 8. The results of the present analysis are compared with those of Mack and Hardee [5] and Astill *et al.* [8]. The comparison indicates an excellent agreement except near the neighborhood of top region of the annuli. In this region, the present results show a slight turn toward the conduction value. The two curves intersect at approximately $Nu_i = Nu_o = 1.099$ and $\theta = 81°$, which coincidentally is the center of the vortex. The transient variation of local Nusselt numbers for $Pr = 0.7$, $R^* = 2.0$, and $Ra = 10^3$, 10^5, and 5×10^5, respectively, are shown in Fig. 9. Examining Fig. 9, we see that the local Nusselt number on the outer surface has a peak near the top of the annulus. The peak value increases with an increase in Rayleigh number.

The relations of average Nusselt numbers on both inner and outer surfaces vs dimensionless time are presented in Fig. 10. In this figure, the solid line represents the inner surface, while the dashed line represents the average Nusselt number for the outer surface. These average Nusselt numbers for the inner and outer spheres $\overline{Nu_i^*}$ and $\overline{Nu_o^*}$ are defined as in equation (12). As time increases, both $\overline{Nu_i^*}$ and $\overline{Nu_o^*}$ approach their steady-state values and should be equal, based on a simple energy balance. In Fig. 10(a), both $\overline{Nu_i^*}$ and $\overline{Nu_o^*}$ approach unity for $Ra = 1 \times 10^3$ as t increases. This means that convection is nearly nil at $R^* = 2.0$ and $Ra = 1 \times 10^3$. As the Rayleigh number increases, the steady state average Nusselt number increases. Figures 10(b) and (c) show the same trend for $R^* = 1.5$ and 1.2, respectively. Average Nusselt number $\overline{Nu^*}$ vs Rayleigh number is plotted in Fig. 11 for a diameter ratio R^* of 2.0. This figure compares our results with results obtained using the equations recommended by Bishop *et al.* [2] and Scanlan *et al.* [3], which were based on experimetal results, and the numerical results of Astill [8] and Singh and Chen [12]. The comparison indicates an excellent agreement between these results.

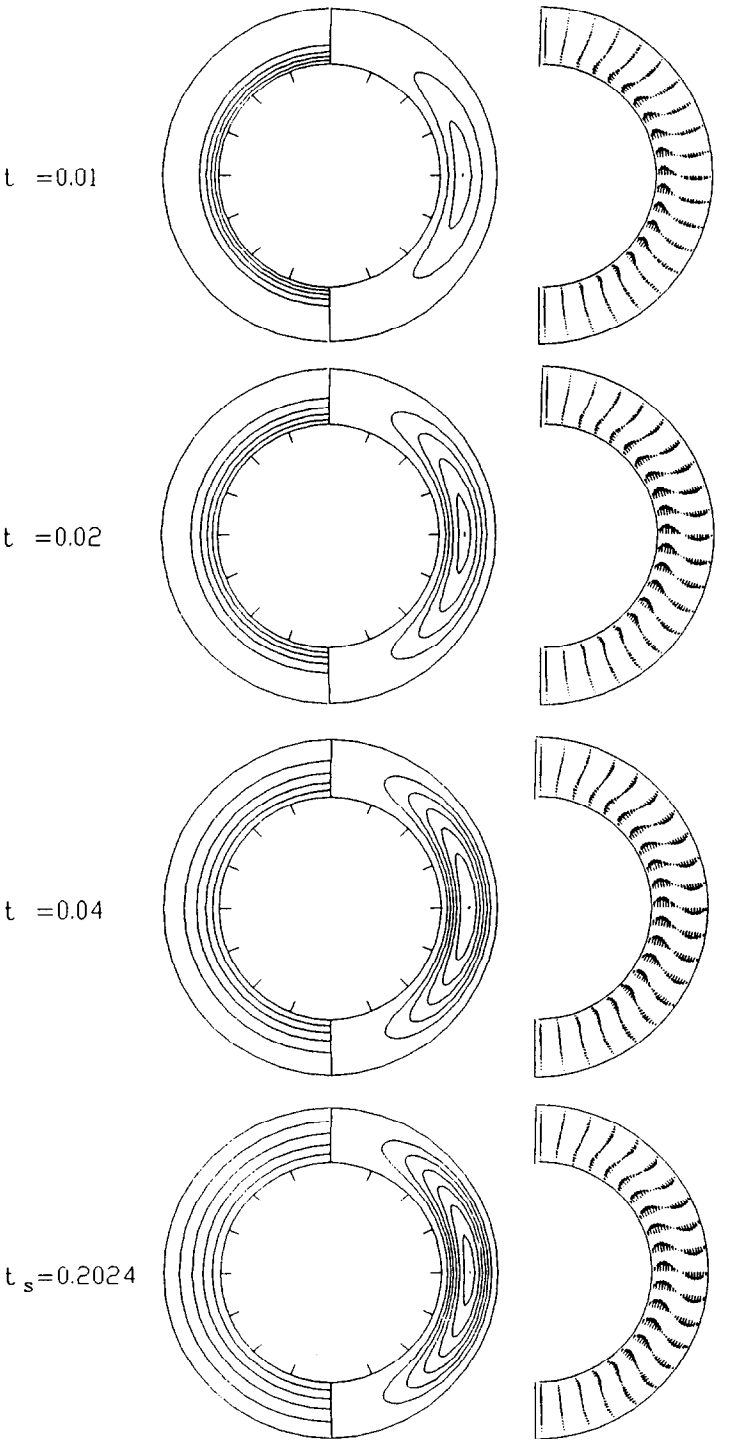

FIG. 4. Streamlines, isotherms, and velocity distributions for $Pr = 0.7$, $Ra = 1.0 \times 10^3$, $R^* = 1.5$ at different time steps. $\Psi_{max} = 0.388$.

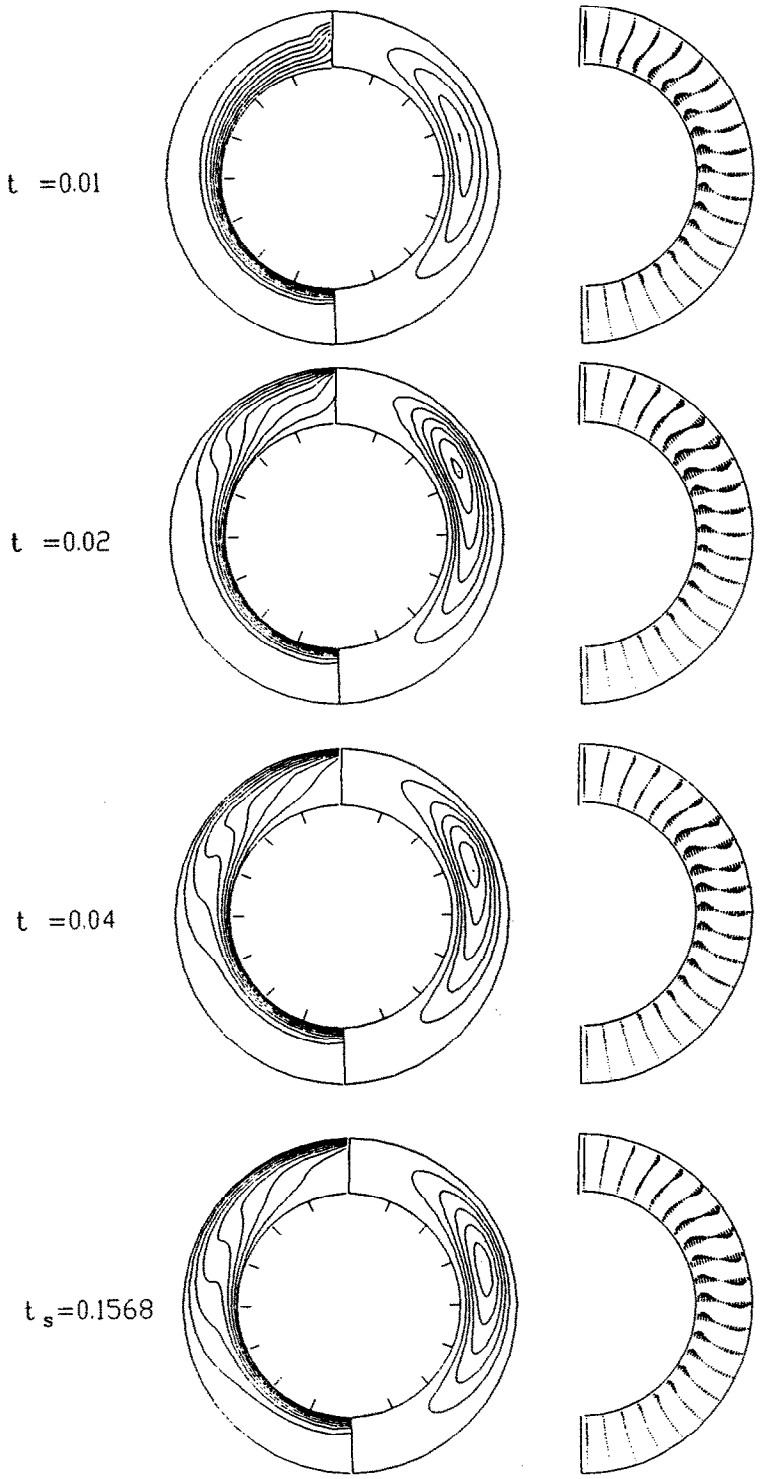

FIG. 5. Streamlines, isotherms, and velocity distributions for $Pr = 0.7$, $Ra = 1.0 \times 10^5$, $R^* = 1.5$ at different time steps. $\Psi_{max} = 22.530$.

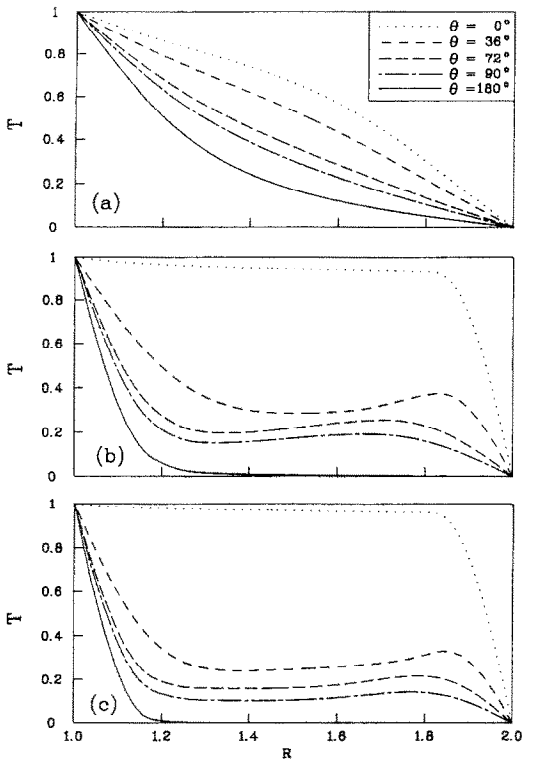

FIG. 6. Steady temperature profiles at various angular positions for $Pr = 0.7$ and $R^* = 2.0$: (a) $Ra = 1.0 \times 10^3$; (b) $Ra = 1.0 \times 10^5$; (c) $Ra = 5.0 \times 10^5$.

CONCLUSIONS

The present work investigates numerically the transient laminar natural convection heat transfer of an incompressible viscous fluid contained between two concentric isothermal spheres. The transient behavior of the flow field and heat transfer is shown graphically. The present results of local and average Nusselt numbers are in good agreement with the results of earlier researchers [2, 3, 5, 8, 12]. Our major results may be summarized as follows: (1) at fixed radius ratio, the average Nusselt number increases with increases in

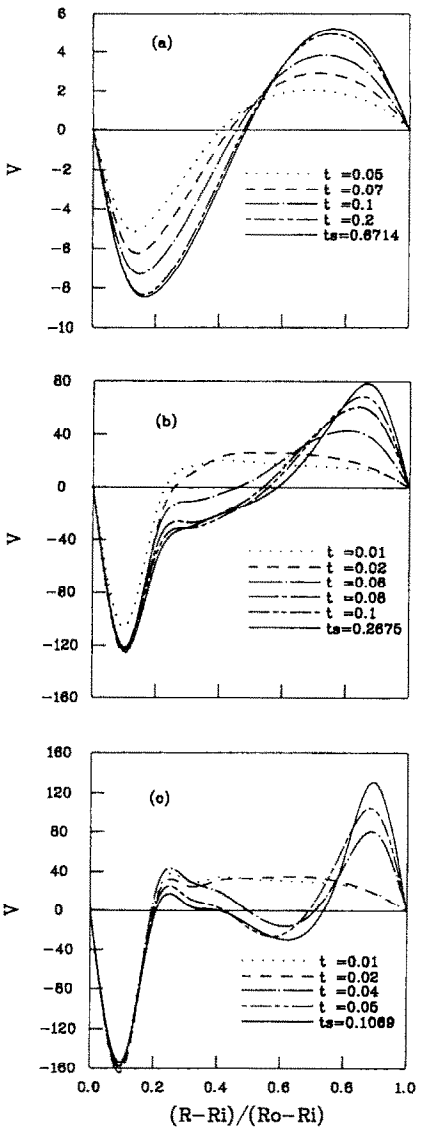

FIG. 7. The transient variations of tangential velocity profiles at $\theta = 90°$ for $Pr = 0.7$, $R^* = 2.0$: (a) $Ra = 1.0 \times 10^3$; (b) $Ra = 1.0 \times 10^5$; (c) $Ra = 5.0 \times 10^5$.

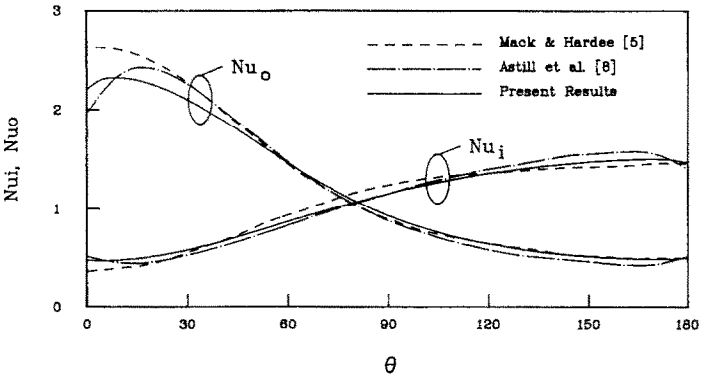

FIG. 8. Variation of local Nusselt numbers on the inner and outer surface at $Pr = 0.7$, $Ra = 1.0 \times 10^3$ and $R^* = 2.0$.

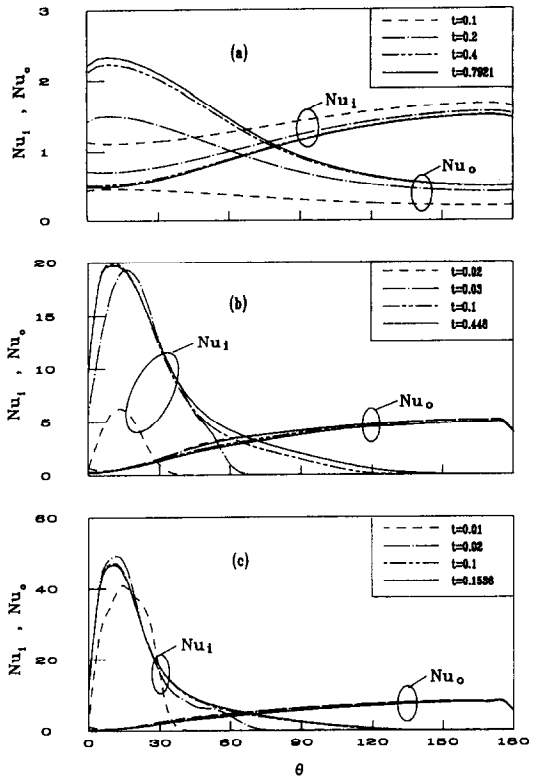

FIG. 9. Transient variation of local Nusselt numbers for $Pr = 0.7$, $R^* = 2.0$: (a) $Ra = 1.0 \times 10^3$; (b) $Ra = 1.0 \times 10^5$; (c) $Ra = 5.0 \times 10^5$.

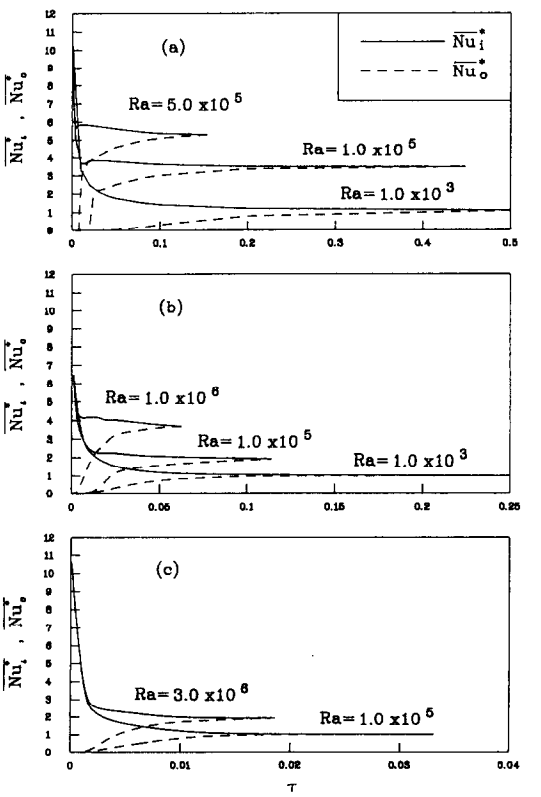

FIG. 10. Temporal variations of the average Nusselt numbers for $Pr = 0.7$: (a) $R^* = 2.0$; (b) $R^* = 1.5$; (c) $R^* = 1.2$.

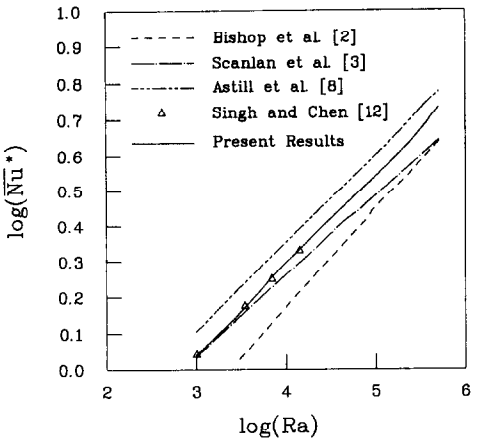

FIG. 11. Steady average Nusselt number as a function of Rayleigh number for $Pr = 0.7$, and $R^* = 2.0$.

Rayleigh number; (2) at fixed Rayleigh number, the average Nusselt number increases with increasing radius ratio; (3) the center of the main vortex (where the value of the stream function is maximum) moves to the upper location with increasing Rayleigh number and radius ratio.

Acknowledgements—The constructive comments of the reviewers are highly appreciated. This research was supported by the National Science Council of the Republic of China through Grant NSC 80-0210-D009-19.

REFERENCES

1. E. H. Bishop, R. S. Kolflat, L. R. Mark and J. A. Scanlan, Convection heat transfer between concentric spheres, *Proc. 1964 Heat Transfer Fluid Mech. Inst.*, Berkeley, pp. 69–80 (1964).
2. E. H. Bishop, L. R. Mack and J. A. Scanlan, Heat transfer by natural convection between concentric spheres, *Int. J. Heat Mass Transfer* **9**, 649–662 (1966).
3. J. A. Scanlan, E. H. Bishop and R. E. Powe, Natural convection heat transfer between concentric spheres, *Int. J. Heat Mass Transfer* **13**, 1857–1872 (1970).
4. S. H. Yin, R. E. Powe, J. A. Scanlan and E. H. Bishop, Natural convection flow patterns in spherical annuli, *Int. J. Heat Mass Transfer* **16**, 1785–1795 (1973).
5. L. R. Mack and H. C. Hardee, Natural convection between concentric spheres at low Rayleigh numbers, *Int. J. Heat Mass Transfer* **11**, 387–396 (1968).
6. R. J. Brown, Natural convection heat transfer between concentric spheres, Ph.D. Dissertation, University of Texas, Austin (1967).
7. E. J. Shaughnessy, J. Custer and R. W. Douglass, Partial spectral expansions for problems in thermal convection, *J. Heat Transfer* **100**, 435–441 (1978).
8. K. N. Astill, H. Leong and R. Martorana, A numerical solution for natural convection in concentric spherical annuli, *Proceedings of the 19th National Heat Transfer Conference*, ASME HTD-Vol. 8, pp. 105–113 (1980).
9. J. P. Caltagirone, M. Combarnous and A. Mojtabi, Natural convection between two concentric spheres: transition toward a multicellular flow, *Numerical Heat Transfer* **3**, 107–114 (1980).
10. J. L. Wright and R. W. Douglass, Natural convection in narrow-gap spherical annuli, *Int. J. Heat Mass Transfer* **29**, 725–739 (1986).
11. A. Mojtabi and J. P. Caltagirone, Natural convection

between two concentric spheres for high Prandtl number, *Proceedings of the Seventh International Heat Transfer Conference, Munchen*, Vol. 2, pp. 245–249 (1982).
12. S. N. Singh and J. Chen, Numerical solution for free convection between concentric spheres at moderate Grashof numbers, *Numerical Heat Transfer* **3**, 441–459 (1980).
13. D. B. Ingham, Heat transfer by natural convection between spheres and cylinders, *Numerical Heat Transfer* **4**, 53–67 (1981).
14. F. Geoola and A. R. H. Cornish, Numerical simulation of free convective heat transfer from a sphere, *Int. J. Heat Mass Transfer* **25**, 1677–1687 (1982).
15. J. S. Huang and S. L. Yang, A finite element solution for natural convection in spherical annuli, *J. CSME* **5**(1), 9–18 (1984).
16. H. Ozoe, H. Kuriyama and A. Takami, Transient natural convection in a spherical and a hemispherical enclosure, *Proc. 1987 ASME–JSME Thermal Engineering Joint Conference*, Vol. 4, pp. 19–25 (1987).
17. Y. Mochimaru, Transient natural convection heat transfer in a spherical cavity, *Heat Transfer–Jap. Res.* **18**, 9–19 (1989).
18. T. Fujii, T. Honda and M. Fujii, A numerical analysis of laminar free convection around an isothermal sphere: finite-difference solution of the full Navier–Stokes and energy equations between concentric spheres, *Numerical Heat Transfer* **7**, 103–111 (1984).
19. H. Ozoe, K. Fujii, T. Shibata, H. Kuriyama and S. W. Churchill, Three-dimensional numerical analysis of natural convection in a spherical annulus, *Numerical Heat Transfer* **8**, 383–406 (1985).
20. M. Fujii, H. Takamatsu and T. Fujii, A numerical analysis of free convection around an isothermal sphere (effects of space and Prandtl number), *Proc. 1987 ASME–JSME Thermal Engineering Joint Conference*, Vol. 4, pp. 55–60 (1987).
21. D. W. Peaceman and H. H. Rachford, Jr., The numerical solution of parabolic and elliptic differential equations, *J. Soc. Indust. Appl. Math.* **3**(1), 28–41 (1955).
22. S. P. Frankel, Convergence rates of iterative treatments of partial differential equations, *Math Tables and Other Aids to Computation* **4**, 65–67 (1950).
23. D. Young, Iterative methods for solving partial differential equations of elliptic type, *Trans. Am. Math. Soc.* **76**, 92–111 (1954).